transferred to the space coordinate $(n+1)\Delta\xi$ where, with a new unused spin packet distribution (consisting at $t'=0$ of the component N_z only), the entire operation was repeated.

[37]The appearance of this oscillatory tail has been noted in many analogous laser calculations. Particular attention is drawn to it in the conclusions of Ref. 27. In Refs. 25 and 26 it is pointed out that it is related to the inhomogeneous broadening of the line.

[38]The gain in energy ($\propto \int s^2\,dt$) is brought about by scaling t to shorter intervals and increasing s.

[39]If we had actually made our earlier calculation using the ten times narrower inverted line we should have deduced a value of only $\sim 10^{-6}$ for s. The margin of error would then have to be $\sim 10\times$.

[40]The evolution of a laser pulse from noise is discussed by J. A. Fleck, Jr., Appl. Phys. Letters 13, 365 (1968).

[41]As pointed out in Sec. III B it is this relatively long phonon lifetime which enables us to obtain approximate analytical solutions for the avalanche burn out.

[42]We were not able to make any reliable determinations of the bottleneck constant σ by observing lattice relaxation in our samples. With the apparatus available it was not possible to obtain uniform initial excitation of the resonance line. Some preliminary tests showed that this deficiency would lead to major errors in the result.

[43]Considerable care was taken to ensure that the sampling fields H_1 were confined to a sufficiently narrow spectral region so that the trace was not distorted by averaging over tanh curves characterized by different values of α_t and $t_{1/2}$. The measurements were made in the center of the burn-out region, and tests were carried out to ensure that the result was not materially affected by any further narrowing of the sampling width.

[44]This is smaller than the gain constants which were estimated in Sec. II B. It is adopted here in an attempt to fit the initial portion of the avalanche curve. As we point out in the next paragraph, the avalanche curve is probably distorted by cross relaxation.

[45]It was found that $(1/M_z)(dM_z/dt)$ decayed exponentially with time in the range from 11 to 25 μsec as suggested by Eq. (4.5). Signal to noise was poor, however, and a fit could equally well have been made to other forms of decay function.

PHYSICAL REVIEW B VOLUME 3, NUMBER 7 1 APRIL 1971

Paramagnetic Resonance and Relaxation of Ce^{3+}, Nd^{3+}, Er^{3+}, and Yb^{3+} in PrF_3

F. J. Rachford and Chao-Yuan Huang
Department of Physics, Case Western Reserve University, Cleveland, Ohio 44106
(Received 4 November 1970)

The electron-paramagnetic-resonance spectra of 1% Ce^{3+}, 1% Yb^{3+}, 0.1% Er^{3+}, and 1% Nd^{3+} in PrF_3 were observed at 4.2 °K. The g factors are found to be $g_x=0.39\pm0.03$, $g_y=0.946\pm0.002$, $g_z=2.69\pm0.02$, $\theta=15.5°\pm0.5°$ for Ce^{3+}; $g_x=2.801\pm0.015$, $g_y=4.48\pm0.03$, $g_z=11.36\pm0.20$, $\theta=41.5°\pm1°$ for Er^{3+}; $g_x=3.47\pm0.03$, $g_y=5.427\pm0.03$, $g_z=1.205\pm0.01$, $\theta=9°\pm1°$ for Yb^{3+}; and $g_x=1.500\pm0.005$, $g_y=1.094\pm0.003$, $g_z=2.937\pm0.017$, $\theta=67°\pm2°$ for Nd^{3+}. The y axis is chosen in the plane perpendicular to the c axis. The other orthogonal axes show no clear relation to the crystal faces, the z axis being rotated θ degrees from the c axis. The hyperfine splitting due to Er^{167} of 47±3 G and due to Yb^{171} of 577±10 G were observed in the y-axis spectra. The spin-bath relaxation rates T_b^{-1} for these same trivalent rare earths PrF were observed in the temperature range $1.3<T<4.5$ °K at frequencies ~8.9 GHz. The Nd^{3+} data were fitted by $T_b^{-1}=2.85T+0.214\times10^{-2}T^9+0.378\times10^{11}e^{-61.5/T}$ (c axis); the Er^{3+} data by $T_b^{-1}=143T+0.125\times10^{10}e^{-56.4/T}$ (x axis showing a strong cross-relaxation first term; the Ce^{3+} data by $T_b^{-1}=0.753T+0.276\times10^{-3}T^9+0.171\times10^{11}e^{-78.3/T}$ (c axis) where an Orbach term $\propto e^{-95/T}$ may also be added, possibly indicating relaxation via the first excited level of Pr^{3+}; and the Yb^{3+} data by single terms proportional to T^2, which is probably due to cross relaxation to pairs.

I. INTRODUCTION

The availability and stable nonhydroscopic nature of the lanthanum trifluorides have lead to their study as possible maser materials. Consequently, electron-paramagnetic-resonance (EPR) and spin-relaxation experiments have determined the rhombic g-tensor components and relaxation mechanisms of trivalent rare-earth ions[1-4] substituted in crystals of LaF_3. Our work extends this investigation to PrF_3,[4] which, like LaF_3, has the tysonite crystal structure.

Three closely related crystal structures have been proposed for tysonite from the x-ray measurements.[5-10] All three are consistent with the Faraday-rotation experiments,[11,12] as interpreted by Van Vleck and Hebb,[10] but fail to account for the crystal-field symmetry observed at the lanthanide site by EPR spectrometry. Recent investigations of the Raman-active phonon modes[13,14] plus the previous EPR observations in LaF_3[1-3] have indicated convincingly that the homomorphic

TABLE I. Principal values of the g tensors of Ce^{3+}, Er^{3+}, Yb^{3+}, and Nd^{3+} in PrF_3. θ indicates the angle between the c and z axes, the y axis being chosen in the plane perpendicular to the c axis. The hyperfine splittings due to Er^{167} and Yb^{171} are also given.

Ion	g_x	g_y	g_z	θ	ΔH_y (G)	A_y (cm^{-1})
Ce^{3+}	0.39 ±0.03	0.946±0.002	2.69 ±0.02	15.5°±5°		
Er^{3+}	2.801±0.015	4.48 ±0.03	11.36 ±0.20	41.5°±1°	74±3	0.0155±0.0006
Yb^{3+}	3.47 ±0.03	5.427±0.03	1.205±0.01	9°±1°	577±10	0.146 ±0.004
Nd^{3+}	1.500±0.005	1.094±0.003	2.933±0.017	67°±2°	Not resolved	

lanthanide trifluorides of the tysonite family share the $P\bar{3}'c'1$ structure. Our resonance work on Kramer's ions substituted in PrF_3 closely follow the results of Baker and Rubens[2,3] on LaF_3 and are consistent with this lattice interpretation.

Spin-lattice relaxation rates of trivalent rare earths substituted in LaF_3 were observed by Schulz and Jeffries[3] (hereafter SJ). Employing similar microwave pulse-relaxation techniques, we observed the spin-lattice relaxation of Ce^{3+}, Nd^{3+}, Er^{3+}, and Yb^{3+} in PrF_3 at low temperatures. What was actually observed were the spin-He-bath relaxation rates; however, since we found no phonon bottlenecking in our samples,[3] we observed spin-lattice rates. Cross relaxation to what may be exchange pairs or other faster-relaxing impurities obscures some of the true rates for the ions in question and is noted where the temperature dependence of the relaxations depart from the expected behavior. In general, for Kramer's ions, we expect the relaxation rate T_b^{-1} due to the Van Vleck–Kronig modulation of the crystalline fields to produce direct, Raman, and Orbach terms:

$$T_b^{-1} = A_1 T + A_2 T^9 + A_3 e^{-\Delta/T}, \tag{1}$$

assuming that the first excited level at Δ is accessible to the phonon spectrum $\Delta < \Theta_D$. In addition, we hoped to see an Orbach term due to the first excited state of Pr^{3+} at $\Delta = 65.8$ cm^{-1} (95 °K).

II. EPR RESULTS

An x-band hetrodyne spectrometer was employed to observe the resonance at ~ 9 GHz and at 4.2 °K. We found that there were six magnetically inequivalent sites with the rhombic g tensors of each site being related to the others by 120° rotations about the hexad (c) axis with accompanying reflections in the plane of rotation.[2]

The PrF_3 samples were prepared by Optovac.[15] Our crystals were aligned by first approximately sighting the c axis between crossed polarizers and then locating the c and a axes by x-ray Laue diffraction. The crystals were cut on a string saw and mounted in our cavity with Duco Cement. These procedures were sufficient to align our crystals to within 3° in our spectrometer. Our crystals were of good optical quality. We noted that cleavage occurred in the c-a plane[4] and that light incident on this plane was reflected "in an almost metallic manner."[2,4]

The spin Hamiltonian for our paramagnetic ions, located at sites of rhombic crystal-field symmetry, is given by

$$H = \mu_B (g_x H_x S_x + g_y H_y S_y + g_z H_z S_z) + A_x S_x I_x + A_y S_y I_y + A_z S_z I_z . \tag{2}$$

The g factors and hyperfine splitting for Ce^{3+}, Nd^{3+}, Yb^{3+}, and Er^{3+} in PrF_3 are presented in Table I.

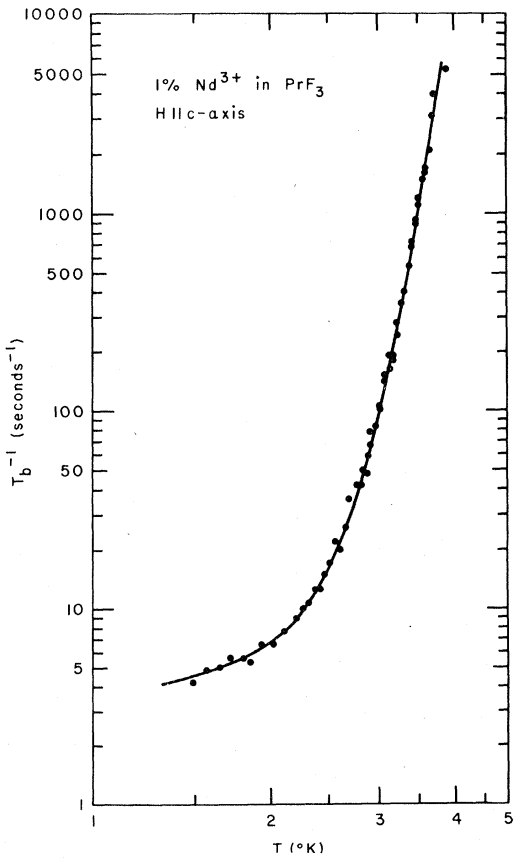

FIG. 1. Spin-lattice data for 1% Nd^{3+} in PrF_3 are fitted by $T_b^{-1} = 2.85T + 0.214\times10^{-2} T^9 + 0.378\times10^{11} e^{-61.5/T}$ for H parallel to the c axis.

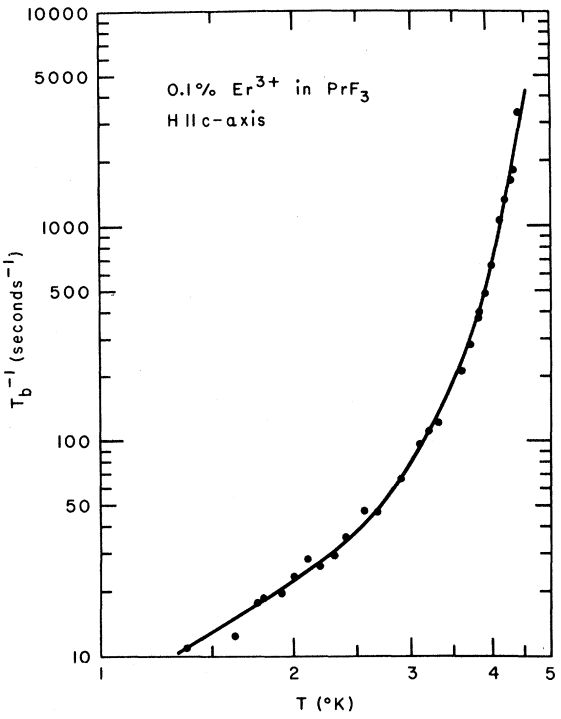

FIG. 2. Spin-lattice data for 0.1% Er in PrF_3 are fitted by $143T+0.125\times10^{10}e^{-56.4/T}$ for H parallel to the x axis.

The y axis is chosen in the plane perpendicular to the c axis. The other orthogonal axes show no clear relation to the crystal faces, the z axis being rotated θ degrees from the c axis.

None of the naturally occurring Ce isotopes possess a nuclear spin and so no hyperfine splitting was observed. Er^{167} has a 30% abundance and has a nuclear spin of $\frac{7}{2}$, and eight hyperfine lines were observed. The splitting along the y axis was found to be $\Delta H_y = 74 \pm 3$ G, which is in close agreement with the $\Delta H_y = 73.5 \pm 2$ G splitting in LaF_3 and the 71.5 ± 0.4 G in $LaCl_3$.[16,17] Assuming negligible mixing of states from higher-J manifolds, we may invoke the theory of Elliot and Stevens,[18] and we may then assume that the ratio A_y/g_y is independent of the particular state and is directly related to μ_I:

$$2\mu_B\mu_N g_n\langle r^{-3}\rangle = a_{4f} = \frac{A_i\langle J\|\Lambda\|J\rangle}{g_i\langle J\|N\|J\rangle}\ , \quad \mu_I = g_n I,$$

for Er $\Delta F_1 \simeq 8000$ cm^{-1} and for Yb $\Delta E_1 = 10\,300$ cm^{-1}. As expected, the splitting is roughly independent of the host crystal.

For Yb^{3+} we observed the $I=\frac{1}{2}$ splitting due to Yb^{171} with $\Delta H_y = 577 \pm 10$ G and $A_y = -0.145 \pm 0.004$ cm^{-1}, as compared to $\Delta H_y = 572.2 \pm 0.5$ G in yttrium acetate[19] and 586 ± 20 G in LaF_3. We could not truly resolve the hyperfine structure of Nd^{3+}, although some structure was seen.

III. SPIN-LATTICE-RELAXATION EXPERIMENTAL RESULTS

A Philco-Ford diode switch was introduced into the spectrometer, providing > 55 dB isolation when switching out the $\frac{1}{2}$-W 9-GHz klystron. The recovery was observed on an Hewlett-Packard model No. 174A oscilloscope and photographed. The time constants were determined by plotting the traces on semilog paper. In order to obtain consistent results, the samples were immersed in the liquid-helium bath and the temperature range (1.3–4.5 °K) was covered by regulating the He-bath vapor pressure. To obtain the functional dependence of the decay rates vs temperature, the simpler log-log plots of the data were fitted by hand, and those involving Orbach processes were fitted by computer using several least-squares programs similar to those of Bevington.[20]

A. 1% Nd^{3+} in PrF_3

Spin-lattice relaxation data taken along the c axis for Nd^{3+} in PrF_3 were well fitted by

$$T_b^{-1} = 2.85T + 0.214\times10^{-2}T^9 + 0.378\times10^{11}e^{-61.5/T}\ \text{sec}^{-1}. \quad (3)$$

The Orbach coefficient is close to the 65 °K first excited level optically determined for Nd^{3+} in LaF_3.[3,21] Our computer program varied the coefficients before the T, $T^9\exp(-\Delta/T)$ terms and also varied Δ. When Schulz and Jeffries[3] (SJ) allowed Δ to be varied in their fitting program, they found $\Delta = 46$ cm^{-1} or $= 66.2$ °K and noted that the energy levels shift with concentration. Our first term is a factor of 3 greater than that of SJ ($0.73T$) and probably is not the true direct rate. Mikkelson and Stapleton[17] observed a direct term of $0.581T$ for Nd^{3+} in $LaCl_3$. The Raman term is slightly less than that of SJ and is believed to represent the true Raman relaxation rate. The fit of our data to Eq. (3) is shown in Fig. 1.

B. 0.1% Er^{3+} in PrF_3

Relaxation data on 0.1% Er^{3+}-doped PrF_3 were taken on the resonances along the x and a axes. The a-axis data were clearly strongly influenced by cross relaxation and were not fitted to a functional form.

Our relaxation data were fitted to

$$T_b^{-1} = 143T + 0.125\times10^{10}e^{-56.4/T}\ \text{sec}^{-1} \quad (4)$$

along the x axis. Certainly, the term $143T$ is due to cross relaxation. Schulz and Jeffries noted a strong concentration dependence for their Er-doped samples. Along the x axis, we find $\Delta = 56.4$ °K which is not close to the SJ value of 72 °K observed in LaF_3. The fit of our data to Eq. (4) is shown in Fig. 2.

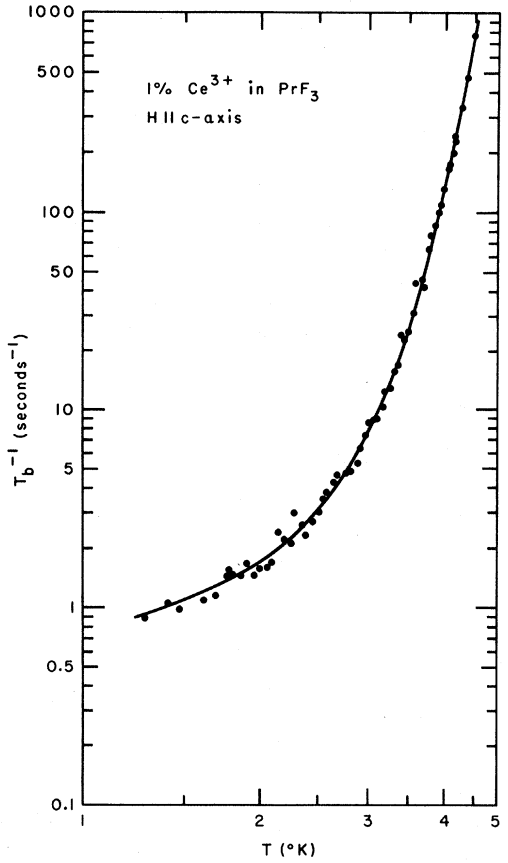

FIG. 3. Spin-lattice data for 1% Ce^{3+} in PrF_3 are fitted by $T_b^{-1} = 0.753T + 0.276\times10^{-3}T^9 + 0.171\times10^{11}e^{-78.3/T}$ for H parallel to the c axis.

C. 1% Ce^{3+} in PrF_3

The spin-lattice relaxation rate of Ce^{3+} in PrF_3 shows the following temperature dependence along the c axis:

$$T_b^{-1} = 0.753T + 0.276\times10^{-3}T^9 + 0.171\times10^{11}e^{-78.3/T}\ \text{sec}^{-1}. \quad (5)$$

Schulz and Jeffries observed relaxation along the c axis and found direct processes of $0.41T$ and $0.28T$ for two different samples doped with nominally 1% Ce^{3+}. They believed the variation to be due to a slight concentration difference. We are probably observing the true direct and Raman processes (SJ find $2.1\times10^{-3}T^9$ in LaF_3). SJ find $\Delta = 56\,^\circ$K along the c axis and attribute this to cross relaxation to Nd^{3+}. We find $\Delta = 78.3\,^\circ$K on the c axis. The first excited state of Pr^{3+} in PrF_3 occurs at $(95\pm1.5)^\circ$K.[22] When we added a second Orbach term forcing $\Delta_2 = 95\,^\circ$K, we found that the computer increased the coefficient before the new exponential till the term was one-seventh the size of the first Orbach term at $4.5\,^\circ$K. Thus, we are able to fit our c-axis data to the equation

$$T_b^{-1} = 0.767T + 0.279\times10^{-3}T^9 + 0.116\times10^{11}e^{-77.1/T} + 0.870\times10^{11}e^{-95/T}\ \text{sec}^{-1}, \quad (6)$$

where the last term may be significant.

The fit of our data to Eq. (5) is shown in Fig. 3.

D. 1% Yb^{3+} in PrF_3

The spin-lattice relaxation of 1% Yb in PrF_3 was fitted to the following expressions:

$$T_b^{-1} = 150T^2\ \text{sec}^{-1}\ (z\ \text{axis}), \quad (7)$$

$$T_b^{-1} = 300T^2\ \text{sec}^{-1}\ (y\ \text{axis}), \quad (8)$$

$$T_b^{-1} = 290T^2\ \text{sec}^{-1}\ (c\ \text{axis}). \quad (9)$$

In all cases cross relaxation to pairs is the probable dominant process. Schulz and Jeffries discuss this process as noted for Yb^{3+} in LaF_3. For our samples, this T^2 dependence is much stronger than that observed by SJ, completely obscuring the T^9 term. Strong cross relaxation of Yb^{3+} has also

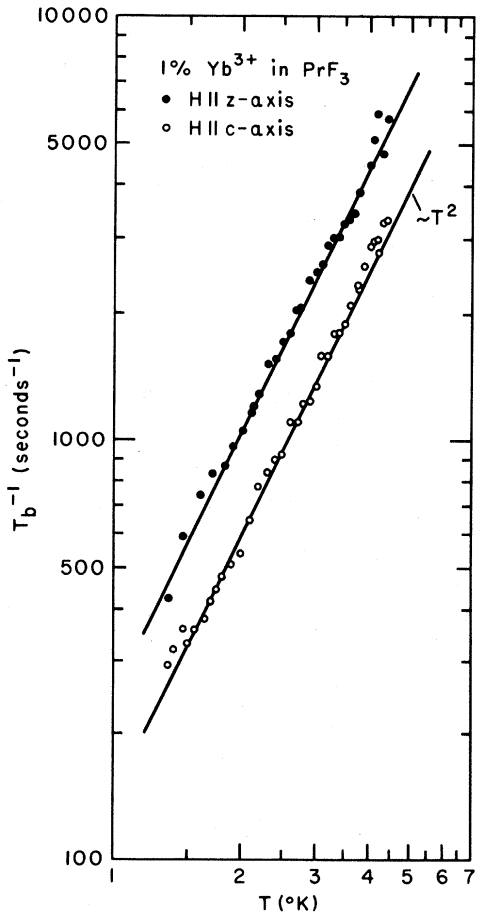

FIG. 4. Spin-lattice data for 1% Yb in PrF_3 indicates a strong T^2 cross relaxation.

been observed by Huang in Yb^{3+}-doped diamagnetic garnets.[23] The T^2 dependence of our data is shown in Fig. 4.

ACKNOWLEDGMENTS

The authors would like to thank Dr. P. Bevington for debugging advice about our computer programs. We are most grateful to Mrs. Su-Lee Huang for her data analysis; and to S. Lin and K. Sugawara for their crystal alignment.

[1]D. A. Jones, J. M. Baker, and D. F. D. Pope, Proc. Phys. Soc. (London) 74, 249 (1959).
[2]J. M. Baker and R. S. Rubens, Proc. Phys. Soc. (London) 78, 1353 (1961).
[3]M. B. Schulz and C. D. Jeffries, Phys. Rev. 149, 270 (1966).
[4]V. K. Sharma, Chem. Phys. Letters 4, 545 (1970).
[5]I. Oftedal, Z. Physik. Chem. (Leipzig) 5B, 272 (1929).
[6]I. Oftedal, Z. Physik. Chem. (Leipzig) 13B, 190 (1931).
[7]K. Schlyter, Arkiv Kemi 5, 73 (1953).
[8]M. Mansmann, Z. Anorg. Allgem. Chem. 331, 98 (1964).
[9]M. Mansmann, Z. Krist. 122, 375 (1965).
[10]A. Zalkin, D. H. Templeton, and T. E. Hopkins, Inorg. Chem. 5, 1466 (1966).
[11]J. H. Van Vleck and M. H. Hebb, Phys. Rev. 46, 17 (1934).
[12]J. Becquerel, W. J. de Haas, and J. Van der Handel, Physica 1, 383 (1934).
[13]R. P. Bauman and S. P. S. Porto, Phys. Rev. 161, 842 (1967).
[14]R. P. Lowndes, J. F. Parrish, and C. H. Perry, Phys. Rev. 182, 913 (1967).
[15]Optovac Inc., North Brookfield, Mass.
[16]C. A. Hutchison and E. Wong, J. Chem. Phys. 29, 754 (1958).
[17]R. C. Mikkelson and H. J. Stapleton, Phys. Rev. 140, A1968 (1965).
[18]R. J. Elliot and K. W. H. Stevens, Proc. Roy. Soc. (London) A215, 437 (1952).
[19]A. H. Cooke and J. G. Park, Proc. Phys. Soc. (London) A69, 282 (1956).
[20]P. R. Bevington, *Data Reduction and Error Analysis for Physical Sciences* (McGraw-Hill, New York, 1969).
[21]H. H. Caspers, H. E. Rast, and R. A. Buchanan, J. Chem. Phys. 42, 3214 (1965).
[22]E. V. Sagre and Simon Freed, J. Chem. Phys. 23, 2066 (1955).
[23]Chao-Yuan Huang, Phys. Rev. 139, A241 (1965).

PHYSICAL REVIEW B VOLUME 3, NUMBER 7 1 APRIL 1971

Energy Distributions for Thermal Field Emission

J. W. Gadzuk and E. W. Plummer
National Bureau of Standards, Washington, D. C. 20234
(Received 16 November 1970)

A sequence of total energy distribution curves for field emission was experimentally obtained for a tungsten emitter heated to 1570 K. Theoretical curves using the Miller-Good WKB-type approximation for tunneling probabilities are in good agreement with the experimental measurements. A significant feature of both sets of curves is a change in slope corresponding to electron emission near the top of the surface barrier where the emission mechanism changes from tunneling to thermionic emission. This feature is in accord with the classical-image force model for the surface potential which appears to be valid for distances approaching 3–4 Å to the metal surface.

I. INTRODUCTION

Measurement of the total energy distribution (TED) of field-emitted electrons[1] is becoming an increasingly powerful method for obtaining information on electron states in and on metals. For instance, studies both experimental[2,3] and theoretical[4] on band-structure effects, virtual electron states in chemisorbed atoms,[3,5] electron-electron interactions,[6] and d-band metal surface states[7,8] have proven to be useful in furthering the understanding of the electronic properties of the materials investigated, and have shown the versatility of the field-emission technique. In this paper we present the first detailed experimental data and analysis of thermal field-emission TED curves in which the details of the surface barrier result in observable and predictable structures in the TED.

II. EXPERIMENT

The experimental measurements were made using a Kuyatt-Simpson–type spherical deflection energy analyzer.[9] The inherent thermal noise in a field emitter[2] was overcome by appropriate signal averaging, using a multichannel analyzer. The field emitter was dc heated at 1570 K (measured by an optical pyrometer) in the presence of an electric field for many hours prior to making a measure-